# The Dependence of the Hydrogen Sorption Capacity of Single-Walled Carbon Nanotubes on the Concentration of Catalyst

**M. Seifi**[a], **D. K. Ross**[b*], **D.J. Riley**[b] **and I. Morrison**[b]

[a]Department of Physics, University of Guilan, Rasht, 41335-1914, Iran.
[b]Institute for Materials Research, University of Salford, Salford, M5 4WT, UK.

**Abstract**

The adsorption of hydrogen on single-walled carbon nanotubes was measured using micro-gravimetric nitrogen and hydrogen adsorption isotherms at 77K for gas pressures of up to 1 bar (nitrogen) and 12 bar (hydrogen). Results show that surface area and hydrogen uptake depend on the concentration of the iron catalyst used for making the nanotubes. Langmuir fits to the hydrogen uptake curves clearly show two adsorption energies for each sample which we attribute to the groove site for the higher adsorption energy and to the convex tube surface for the lower energy. We also present calculations of the binding energy of hydrogen on these same sites on SWCNTs and confirm that the groove site has a significantly higher (radius-dependent) binding energy than the surface site, consistent with the experimental values. This suggests that the use of the Langmuir model is appropriate to the adsorption of H2 on activated carbons for the temperature and pressure range investigated and could be used as a rapid way of estimating the average tube radius in the sample.

## 1. Introduction

Single-Walled Carbon Nanotubes (SWCNT) provide a useful model system for investigating the $H_2$ –surface interaction - in particular on graphitic surfaces. The measurement of gas adsorption isotherms – specifically for $H_2$ and $N_2$ - provides a direct way of characterising the surface area and pore size distribution in porous materials. The method can cover a wide range of pore sizes from 0.35 nm up to >100 nm. The amount of gas adsorbed on a solid depends on temperature and gas pressure

*Corresponding author. Fax: 0044 161 2955147; d.k.ross@salford.ac.uk

and on the interaction energy between the adsorbate and the solid surface. There are two main ways in which hydrogen can be adsorbed on a material surface - physisorption and chemisorption. In physisorption, $H_2$ keeps its molecular identity whereas in chemisorption, the molecule dissociates and hydrogen is stored in its atomic form prior to possible further interactions [1]. Hydrogen physisorption on carboneous materials is normally due to Van der Waals interactions between the surface carbon atoms and the hydrogen molecules [2]. Hydrogen physisorption on bundles of single-walled carbon nanotubes (SWCNTs) is maximised when the nanotubes are arranged so as to produce highly uniform micropores sizes, high surface areas and a relatively strong attractive surface potential [3]. The bundles of SWCNT offer at least three different kinds of adsorption sites: grooves sites, above the lines along which two tubes in the outer surface of the bundle touch; the outer surface of individual tubes; and the interstitial channels (ICs), the space formed by three tubes in the interior of bundle. Hypothetically, if the SWCNT‘s are open-ended, a further type of adsorption site would exist within the interior of a tube [4].

In a previous paper, we reported on inelastic neutron scattering from para-$H_2$ adsorbed on a different sample of nanotubes, mainly at 20K [5]. These results suggest that there are two types of site. If the molecule is only weakly trapped, we expect a peak in the inelastic scattering at 14.7meV due to stimulating the molecule from the J=0 to J=1 rotational level. An interaction with the surface will tend to lower this energy due to a resulting increase in the H-H distance and corresponding reduction in the angular momentum of the molecule. An ellipsoidally shaped interaction potential will split the level into m=0 and m=+/-1 states. Because the scattering from $H_2$ on the first site to be occupied shows a split peak, it can be concluded that the potential at

this site is strongly perturbed from a spherical form as would be expected for the groove sites. At higher coverage, a third peak appears at around 14.7 meV, suggesting scattering from weakly trapped hydrogen molecules in a spherically symmetric potential while at higher coverage still, a further single peak appears at a slightly lower energy. The conclusion reached in this paper was that the first site to be occupied is the "groove" site where a strongly perturbed potential is to be expected while the second site is on the convex external surface. When this surface is completely covered, a second $H_2$ layer begins to form (possible because the temperature is below the critical point for $H_2$), pressing the first layer closer to the tube surface and causing the peak in the scattering due to the covered molecules to drop to a slightly lower energy level due to the stronger interaction with the surface. This conclusion as to the two sites occupied is now generally accepted [6].

In a subsequent investigation [7], we produced SWCNT by a CVD method and investigated the range of tube diameters produced using Raman scattering. The CVD method employed involved passing a hydrocarbon gas over suitable catalytic particles (2% by weight Fe) on an inert substrate. The results showed that the surface area was influenced by the catalyst particle density, the lower density giving a larger surface area. It should be noted that during the CVD process, the catalyst particles become coated with amorphous carbon so that spillover catalysis cannot contribute to the interaction between hydrogen and sample. In the present paper, we report micro-gravimetric measurements of the adsorption of nitrogen and hydrogen on two samples of SWCNTs produced by this method but with different densities of catalyst particles. These measurements allow us to evaluate the specific surface areas (BET) and the $H_2$ storage capacities of the samples and also to derive information about the diameter of

the pores in the samples, by analysing the hysteresis loop in the $N_2$ isotherm. On the assumption that the surface area of the material is dominated by the nanotube content, its purity can be estimated from the BET surface area. It is also possible to estimate the energy of adsorption and the relative population of hydrogen on the two types of site by fitting the observed isotherm using a Double Langmuir model.

In order to test our assumption that the more strongly adsorbing sites are along the line of the grooves and the less absorbing sites are on the convex surfaces of individual nanotubes, we have performed Density Functional Tight Binding calculations of the relative adsorption energies as a function of the tube diameter using the method described by Aradi et al [8]. It is well known that normal density functional methods have difficulty in dealing with the long-range Van der Waals interactions involved in the present case. This difficulty has been dealt with using the method proposed by Elstner et al [9]. Full details of this method will be published later [10]

**2. Experimental technique**

Magnesium Oxide[1] (MgO) was used as the catalyst support and Fe (in two different concentrations) as the catalyst. The catalyst materials for our CVD process were prepared by the method described in detail previously [6]. Here the first sample contained 1.5 wt% Fe and the second, 2.2 wt% Fe. Images of the samples produced using an SEM (JOEL JSM 6400), and a TEM (JEOL 3010) show large numbers of bundles of nanotube distributed throughout samples. These images also show the

[1]Fisher Chemical (www.fisher.co.uk )

presence of carboneous material in the samples. Raman scattering with different incident wavelength radiations (488, 514.8 and 632.8 nm) was used to establish the electromagnetic response of the samples, from which the distribution of tube diameters could be estimated. These measurements showed that the SWCNT in both samples are predominantly semiconducting with diameters in the range from 1.10 to 1.45nm [7].

Here we report micro-gravimetric measurements of nitrogen and hydrogen adsorption at 77K and for gas pressures of up to 1Bar (nitrogen) and 12Bar (hydrogen) using an Intelligent Gravimetric Analyser (IGA) from Hiden Isochema[2]. These measurements were used to evaluate the specific surface areas (BET) and $H_2$ storage capacities of the samples. They were performed on 148mg (1.5% Fe) and 162mg (2.2% Fe). Prior to the adsorption measurements, samples were degassed in the IGA chamber for a period of 16 hours in a vacuum < $10^{-6}$ Torr and at successive temperature stages up to 450ºC. It has previously been shown [5] that this careful out-gassing process is essential to attain the full surface area. Following the adsorption measurement, a desorption measurement was made to ensure that the mass returned to the degassed value, indicating that the sample had not adsorbed impurity gases from the apparatus.

## 3. Results

### 3.1 *Nitrogen adsorption*

Nitrogen adsorption and desorption isotherms were performed on the samples at different degassing temperatures up to 450°C. It was found that on increasing the

[2] Hiden Isochema (www.hidenisochema.com )

degassing temperature from room temperature up to 450°C, the surface area of the samples increased but not by very much. The nitrogen adsorption and desorption isotherms and the corresponding BET plots for the samples at 77K following degassing at 450°C are shown in Fig 1. This figure shows the quantity of nitrogen taken up /g of samples. Both isotherms are Type IV with a hysteresis loop at pressures higher than 0.4 bar. The surface area derived from the BET plot for the 1.5% Fe sample (350 $m^2/g$) is higher than for the 2.2% Fe sample (227 $m^2/g$). We would suggest that this difference results from the different concentration of catalyst in the

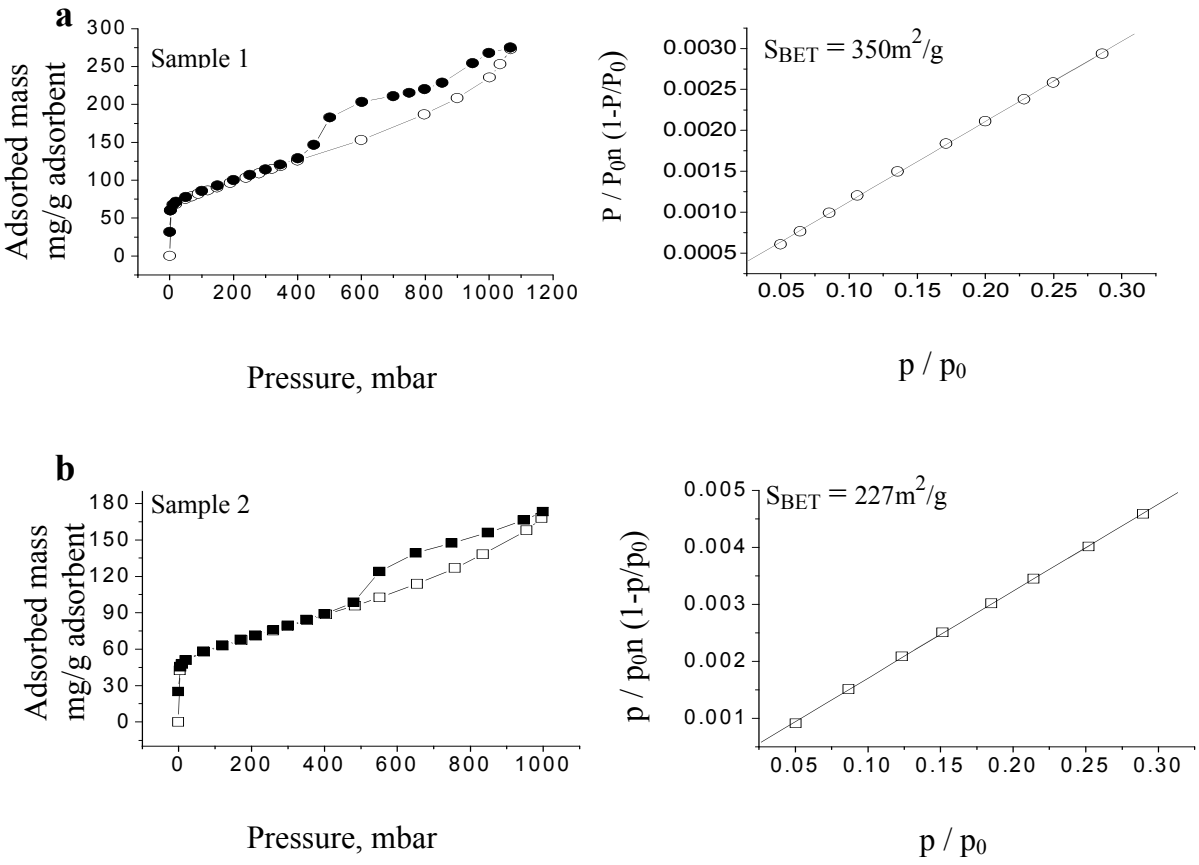


Figure 1. Nitrogen adsorption and desorption isotherms for both samples at 77K following degassing at 720K: (a) sample 1, adsorption (open circles) and desorption (filled circles) with a corresponding surface area of 350 $m^2/g$; (b) sample 2, adsorption (open squares) and desorption (filled squares) with a corresponding surface area of 227 $m^2/g$.

two samples. Larger concentrations of Fe might be expected to produce fewer nanotubes if the Fe particles are close together and tend to aggregate. These large particles can then easily become encapsulated with excess carbon and hence will be completely inactive [11]. Analysis of the hysteresis loop allows us to derive information about the diameter of pores in the sample using the t-plot method [12]. Here Equation (1) is the Kelvin Equation, defining the partial pressure over a meniscus of radius, $r_k$,

$$\log \frac{p}{p_0} = \frac{-4.14}{r_k} \tag{1}$$

Equation (2) is the so-called t plot, a statistical thermodynamics representation of the variation of the thickness of the multilayer coverage, t, as a function of $p/p_0$ which enables us to plot the measured mass uptake against t

$$\log \frac{p}{p_0} = 0.034 - \frac{13.99}{t^2} \tag{2}$$

from which Equation (3) gives the radius of the pore.

$$r_p = r_k + t \tag{3}$$

Here, $p_0$ is the saturation vapour pressure, $r_k$ is the inner radius of the wetted pore and $r_p$ is the radius of pore. In the absence of pore filling, the t-plot would be a straight line through the origin. A downward bend in the plot with increasing t indicates pore filling. From the range in $t$ over which the bend takes place and the corresponding values of $p/p_0$ and hence of $r_k$ the corresponding range in pore diameter can be obtained. For both samples, this turns out to be in the range from 3nm to 8nm. The lower limit of radius could be attributed to some large open-ended nanotubes or to defect structures in the bundles, whereas the larger extreme of this distribution might be due to bundles of tubes interlacing with each other.

3.2 *Hydrogen Adsorption*

Hydrogen gas adsorption isotherms were measured for both samples at pressures up to 12 bars at 77K. The adsorption curves are typical of Type I isotherms. At 12 bar pressure, the higher hydrogen adsorption capacity was found for the 1.5% Fe sample namely 0.5 wt% $H_2$ while the 2.2 wt% Fe, adsorbed 0.25 wt% $H_2$. Figure 2 gives a comparison of the hydrogen isotherms obtained for the 1.5% and 2.2% Fe samples. Figure 2(a) is plotted on a linear $p/p_0$ scale and Figure 2(b) is on a double logarithmic plot, to emphasise the low $p/p_0$ region. Because there is generally a linear relationship between the hydrogen storage and the specific surface area [13], the 1.5wt% Fe sample, with the higher BET surface area, should take up more hydrogen per gram, as is indeed observed.

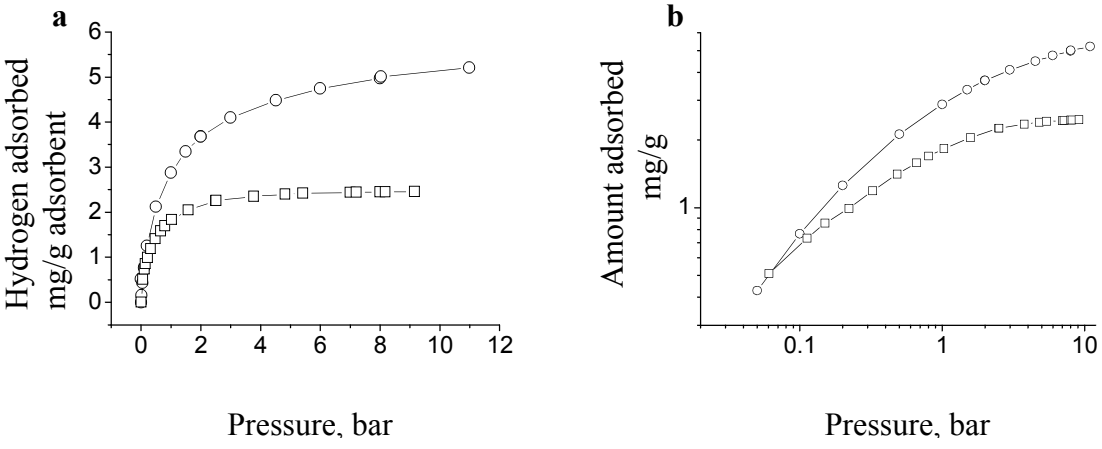


Figure 2. Adsorption isotherms for hydrogen on 1.5 wt% Fe sample (circles) and the 2.2 wt% sample (squares). Isotherms are plotted on a linear scale in (a) and on a double-logarithmic scale in (b) to emphasise the low pressure part.

When the isotherms are plotted on a double-logarithmic scale, the low pressure region is magnified. Figure 2 (b) shows that at low pressures, up to about 50-60 mbar, the

isotherms of both samples are similar but, for higher pressures, the 1.5 wt% Fe sample takes up

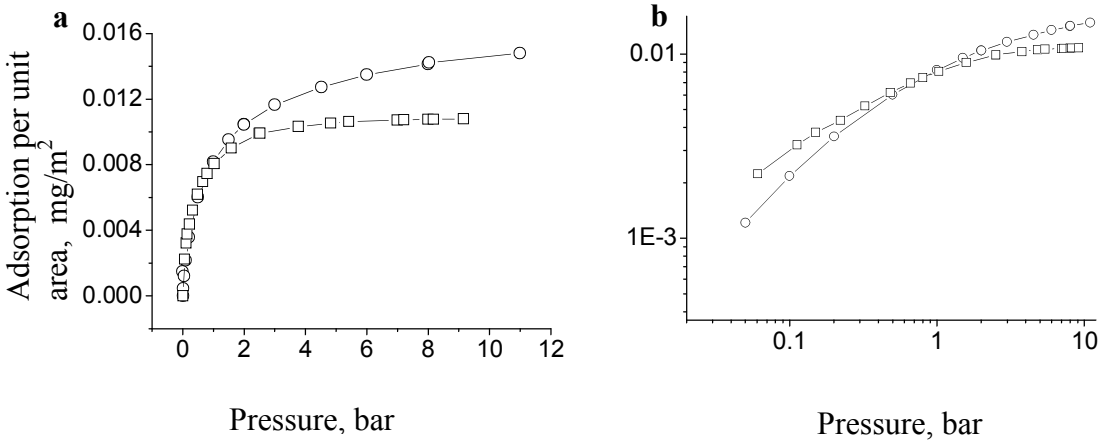


Figure 3. Hydrogen storage densities of sample 1 (circles) and sample 2 (squares) normalised to the measured BET surface areas as a function of pressure. (a) for linear scale and (b) for a double-logarithmic scale

more hydrogen. In Figure 3, the hydrogen adsorption of both samples has been normalized to the surface area as measured from the nitrogen adsorption isotherm using the BET method [14]. On the double-logarithmic scale, Figure 3b, it can be seen that at about 0.7-1 bar the isotherms for the two samples cross. The hydrogen density on the 2.2wt% sample is higher at pressures below 0.7 Bar and vice versa. The reason for this behaviour is presumably that sites with higher heats of adsorption are present in a greater concentration on the surface of this sample whereas the 1.5 wt% sample has a greater concentration of the lower energy sites. Figure 4 shows the coverage of samples against chemical potential, where the data are fitted with an isotherm in a Fermi-Dirac (Langmuir) form, for a unique site energy, ε [15].

$$\theta = \frac{1}{\exp\frac{\varepsilon-\mu}{KT}+1} \qquad (4)$$

Here θ is the fractional occupation of a given site type, ε is the adsorption energy of these sites and μ is the chemical potential. A first approximate fit was obtained for an assumed single site energy of 53meV (1.5 wt % Fe) and 58meV (2.2wt% Fe). It is clear, however, that this single Langmuir model does not produce a good fit to the data, presumably because there is a distribution of sites energies.

Clearly one could fit these data with a variety of distribution functions for the site energy. However, a two-site distribution was preferred because, as reported above, the inelastic neutron scattering (INS) measurements on Carbolex SWCNTs [5] show a spectrum that is clearly due to a combination of two different types of sites. The resulting double-Langmuir fits (Figure 5) show that one of the two sites (presumably the "groove" site) is significantly more strongly adsorbing.

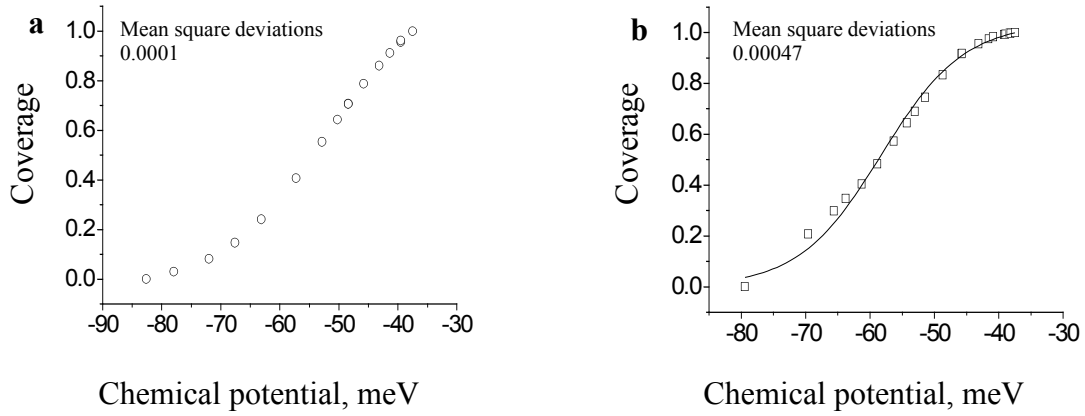


Figure 4. Adsorption data for hydrogen (open circles) plotted against chemical potential compared with the fit to Equation (4), yielding a single trapping energy of (a) 53 meV (1.5 wt % Fe) and (b) 58 meV (2.2wt % Fe).

For this model, with site energies $\varepsilon_1$ and $\varepsilon_2$, the Fermi-Dirac (Langmuir) equation can be written:

$$\theta = a\frac{1}{\exp\frac{\varepsilon_1-\mu}{KT}+1} + (1-a)\frac{1}{\exp\frac{\varepsilon_2-\mu}{KT}+1} \qquad (5)$$

Here a and (1-a) are the fractions of the available sites with adsorption energies of $\varepsilon_1$ and $\varepsilon_2$ respectively. The fitted values are given in Table 2 where the quoted errors are values given by the fitting routine. The fit for 1.5 wt% Fe sample gives 39.1meV with a concentration of 60% for the lower energy site and 53.3meV with a concentration of 40% for the higher energy site while the 2.2wt% Fe sample gives 47.7meV with a 70% concentration for the lower energy site and 60.8meV with a concentration of 30% for the higher energy site. It will be seen from the values of the mean square deviations that the two-Langmuir form gives a much better fit to the data. In agreement with [16], assuming that the hydrogen adsorption occur on the groove and surface sites on the exterior of the nanotube bundles, we attribute the smaller value of the isosteric heat of hydrogen adsorption to the surface sites and the larger value to the groove sites. We would note that, as shown in Figure 3, at low pressures, the adsorption in the 2.2wt% Fe sample exceeds that in the 1.5wt% Fe sample because the heat of adsorption in the groove sites is higher in this sample even though a smaller proportion of sites are of this type for this sample.

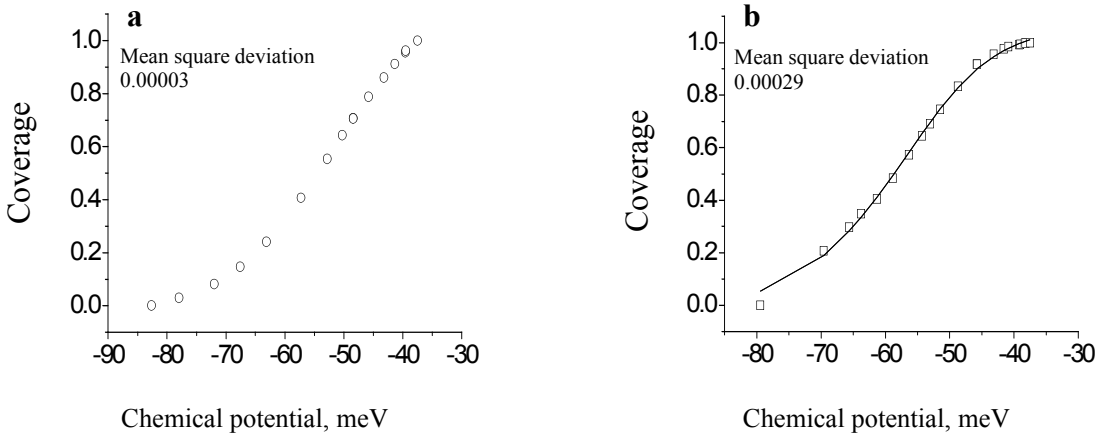


Figure 5. Data for adsorption of hydrogen plotted against chemical potential and fitted with a two-site Langmuir (Equation 5) for (a) the 1.5 wt % Fe sample with heats of adsorption of 53.3 and 39.1 meV and (b) the 2.2 wt % Fe sample with heats of adsorption of 60.8 and 47.7 meV.

Surface areas and corresponding storage capacities and isosteric heats of adsorption for the samples are summarized in Table 1.

Table 1. BET Surface Areas, Hydrogen Adsorption (wt%) and fitted heats of adsorption using the Double Langmuir model for the nanotube samples

| Sample | Surface area, $m^2/g$ at 77 K | Storage capacity wt% at 10 bar | Isosteric heat of adsorption meV/$H_2$ | Proportions stored in each site, % |
|---|---|---|---|---|
| 1.5 wt % Fe | 350 | 0.5 | -53.3 ±0.8<br>-39.1 ±1.2 | 40<br>60 |
| 2.2 wt % Fe | 227 | 0.25 | -60.8 ±4.8<br>-47.7 ±1.8 | 30<br>70 |

3.3 *Calculated binding energy of hydrogen molecules in groove and surface sites*

As mentioned above, Density Functional Tight-Binding (DFTB) calculations have been carried out on various single-walled carbon nanotube structures using the method described by Aradi et al [8] to determine the binding energies of $H_2$ molecules in relevant geometries. Due to the weak nature of the binding both between the tubes and between tubes and a hydrogen molecule, a Van der Waals interaction correction has been introduced. This correction has been implemented using a Slater-Kirkwood type model as described by Elstner et al [9]. These authors have shown that this approach avoids the known deficiencies of the LDA and GGA treatments when used with Density Functional Theory which respectively over- and under-estimate the van der Waals binding energy. The minimum energy positions for hydrogen binding both normal to the tube surface and along the groove between pairs of touching tubes have been established by performing energy calculations with the $H_2$ displaced at 0.1 Å intervals from the starting position. For the surface calculations, the displacements are measured from the surface of the tube along a radial direction and, for the groove site, from the mid-point between the tubes along a tangential direction. In both cases, the

molecule was centred over the middle of a carbon hexagon. The energy value quoted is for the molecular axes lying as shown in Figure 6. These orientations were chosen because they showed the lowest minimum energy of those tested. In order to estimate the true adsorption energy, it is necessary to subtract the zero point energy.

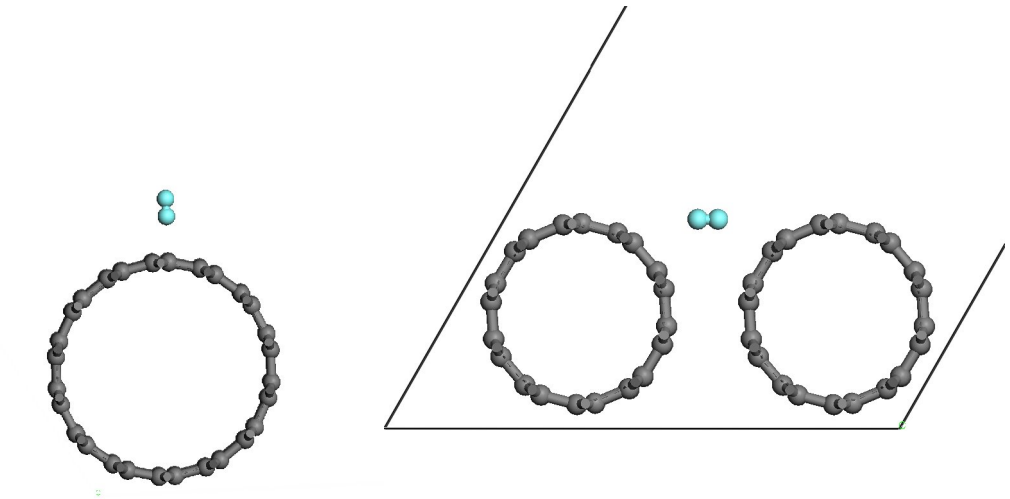

Figure 6. Diagrams of the orientations of the $H_2$ molecules for which the calculations were preformed for (a) the surface sites and (b) the groove site

This was calculated by fitting a parabola to the bottom of the potential well both normal to and parallel to the surface. The results of these calculations are given in Table 2 and are plotted in Figure 7 showing a systematically stronger binding in the groove site compared to the surface site. The calculations have been repeated for a number of different tube geometries, namely (5,5), (7,7) and (10,10) which are typical of the distribution of tube diameters observed in a similar sample from Raman measurements of the radial breathing mode frequencies [7]. Figure 7 also indicates an increase in the binding energy of the groove site as a function of increasing tube radius, although with some further dependence on the chiral geometry. The effective binding energy for the surface sites varies less with no systematic trend. The results show that the ratio of the effective binding energy in the groove site to that in the

surface site increases from 60% to 77% as the diameter of the SWCNTs increases for the tube geometries calculated.

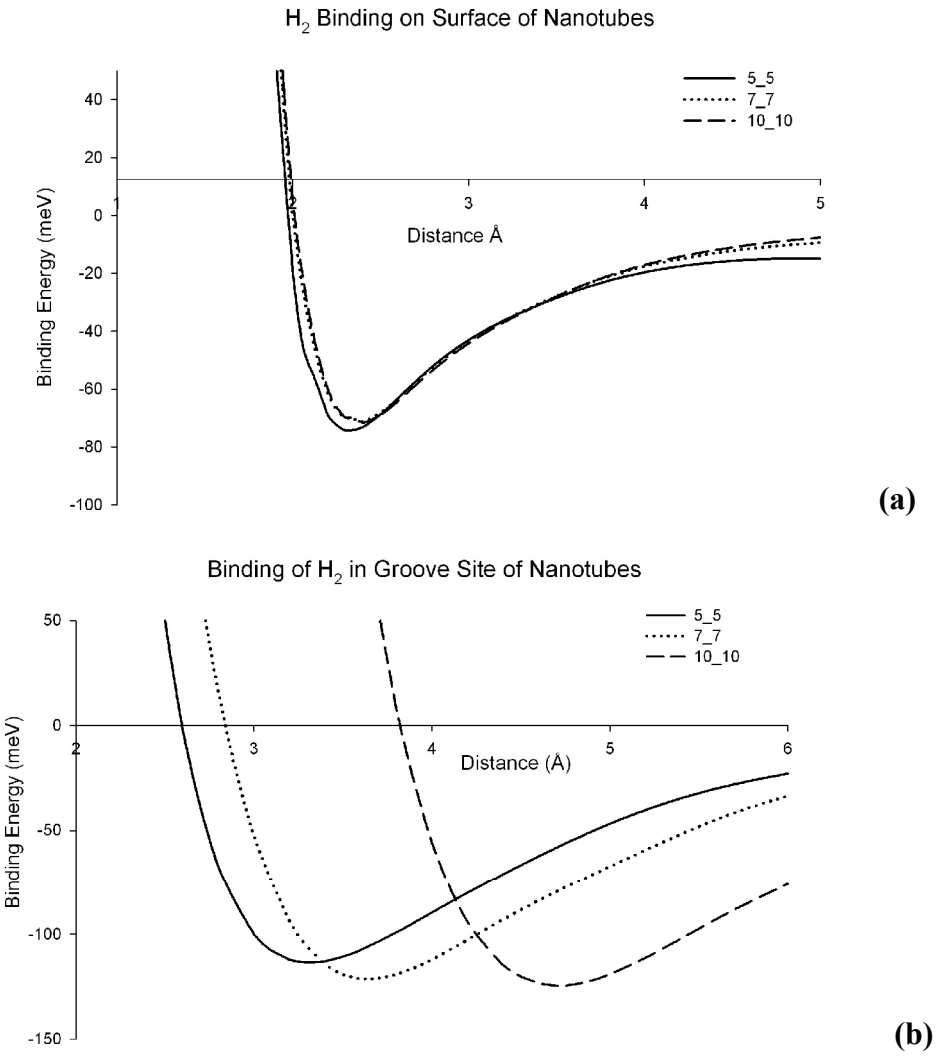


Figure 7. Calculated binding energy of hydrogen molecules as a function of molecule position for single-walled carbon nanotubes for (a) surface sites and (b) groove sites

It will be noted that the calculated effective trapping energies are somewhat less than the observed values given in Table 1 and also that the measured ratios of groove site to surface site binding energies are lower (the 1.5wt% Fe sample, 136% and the 2.2wt% Fe sample, 127%). It is interesting to note that the higher wt% Fe sample has the higher trapping energy on the groove site and hence presumably the larger average tube diameter. Obviously, the larger the tube radius, the smaller the proportion of groove sites to surface sites – which is consistent with the trend in the relative surface

area of the two sites obtained from the Double Langmuir fits (Table 1). However, it should also be noted that the 2.2wt% Fe sample shows a significantly higher adsorption energy for the surface sites than does the 1.5 wt% Fe sample, whereas the calculations suggest that the trapping energy for the surface site should be fairly independent of radius.

Table 2. Calculated binding energies of $H_2$ on different nanotube configurations. The Effective Binding Energy is the Binding Energy less the Zero Point Energy.

| Tube/Site | Binding Energy (meV) | Zero Point Energy (meV) | Effective Binding Energy (meV) |
|---|---|---|---|
| **5_5 Groove** | 113.54 | 24.47 | 89.07 |
| **7_7 Groove** | 121.21 | 29.78 | 91.43 |
| **10_10 Groove** | 124.54 | 24.88 | 96.66 |
| **5_5 Surface** | 74.30 | 18.40 | 55.90 |
| **7_7 Surface** | 71.35 | 14.91 | 56.44 |
| **10_10 Surface** | 71.67 | 15.43 | 56.24 |

## 4. Discussion of results

It is now well established that there are two trapping sites for hydrogen on SWCNT samples. The inelastic neutron scattering data provides very specific evidence for a more strongly adsorbing site with an energy splitting typical of an oblate distortion of the trapping potential. Subsequently, Panella et al [6] using thermal desorption mass spectrometry showed two well separated desorption maxima , a sharp peak at 34K and a rather broader peak around 51K. Although these peak temperatures cannot be directly related to a binding energy, as the peak position depends on the heating rate, the ratio of the observed desorption temperatures is 1.5, intermediate between the present experimental and calculated ratios for the ratio of the adsorption energies. The SWCNT sample used in these measurements was produced by the HiPco method [17] and so probably has a wider range of tube radii [7]. These authors set out the

arguments for concluding that there is no hydrogen trapped inside the tubes or in the internal interstitial spaces and that therefore the lower trapping energy refers to the external convex surfaces and the higher trapping energy to the groove sites. Further evidence for the two trapping sites has been obtained by Panella et al, using Raman scattering [18]. The Raman technique measures the H-H stretching frequency associated with different J values, the Q(J) lines. For $H_2$ trapped on a surface site, these frequencies are shifted slightly upward (in contrast to the pure rotational levels measured by neutron scattering which show a reduction in energy due to the increase in the H-H distance [5]. For hydrogen on the HiPco sample, this technique shows two distinct peaks due to two different trapping sites in addition to the free molecule peak which appears at high hydrogen pressure.

Several authors have published predictions of the trapping energy of $H_2$ molecules on plane graphene surfaces and on external curved surfaces of nanotubes with which our results can be compared. There are three approaches used in the literature, the use of empirical potentials associated with Grand Canonical Monte Carlo calculations to simulate total absorption as a function of temperature and pressure, the DFT calculations, which have to deal with the long-range van der Waals forces present here (which are over-estimated by the LDA method and underestimated by the GGA method) and the more elaborate but accurate molecular orbital method which can only be applied to a single molecule. Using the first technique, Williams and Eklund [19] calculated that the groove site would have a trapping energy of 93.8 meV and the surface site would be 46.7 meV, rather higher than the experimental values. Using the DFT method, the potential energy surface has been plotted with the $H_2$ axis normal to the graphene plane over the centre of the hexagon. However, to the best of

our knowledge, no calculations have been published for the corresponding trapping energy of $H_2$ in the groove site. Thus, Henwood and Carey [20] have carried out DFT calculations for both graphene layers and internal and external sites on (9,0) and (10,0) single-walled nanotubes with the $H_2$ axis orientated both parallel and perpendicular to the nanotube surface. For the site specified (i.e for the B site, as designated in their paper), these authors report maximum binding energies for graphene of 86.83 meV for LDA and 22.17 meV for GGA. Cabria et al [21] also report DFT/LDA calculations for an $H_2$ molecule at the same site for graphene of 89 meV, in remarkable agreement with the 86.83 meV reported above. The third approach is to perform accurate molecular orbital theory which should get the binding energy more or less exactly correct. However, this approach is much more computationally intensive and only works for molecules (not for a periodic structure). It is therefore necessary to make the calculations for $H_2$ on molecules such as $C_{24}H_{12}$ [22]. This calculation yields a binding energy of 90.78 meV, close to the LDA results. On going from the graphene sheet to the external surface of a nanotube, we would expect the maximum binding energy to be somewhat reduced and this is confirmed by Henwood and Carey[20]. In their calculations, for a (10,0) tube, LDA gives binding energies of 79.20 meV and GGA gives 20.70 meV. For a (9,0) tube, LDA gives 79.75 meV and GGA gives 20.78 meV. As would be expected, our results, before removing the zero point energy, are just below the Henwood and Carey LDA values for all tubes considered. These considerations lend considerable support to our present calculations so that we can be confident that our values for the groove sites can be relied on. We can thus conclude that the more strongly adsorbing sites can be identified with the groove sites. Moreover, the calculated excess of the groove site binding energy as compared to the external curved site energy is rather more than the

value extracted from the data (50% increase for the smallest diameter (5,5) tubes compared with 33% averaged over the two samples). This suggests that the samples may consist of SWCNTs containing tubes of a somewhat smaller average diameter.

Both the $H_2$ isotherm measurements and the first principles calculations thus confirm the result of the inelastic neutron scattering experiments reported earlier [5], namely that the $H_2$ molecules are adsorbed on two types of site. The first, more strongly adsorbing, (groove) site has a distorted spherical potential in which the J=1 state splits into two (m= +/-1) levels both shifted downward in energy and one (m= 0) level shifted upward while the second site is essentially unperturbed.

The ability of the Double Langmuir fit to confirm the existence of two different types of site with different trapping energy with high accuracy makes it a useful way to analyse adsorption of $H_2$ on carbon surfaces in the current pressure/temperature range. Where a carbon surface has a distribution of site energies, appropriate distribution functions can be used to characterise the surface.

**4. Conclusions**

Nitrogen adsorption and desorption isotherm measurements were performed on two samples at 77K. The resulting BET surface area for the 1.5wt% Fe sample is 350 $m^2/g$ and for the 2.2wt % Fe is 227 $m^2/g$. This difference could result from the different concentration of catalyst in two samples. Catalyst particles (here Fe) present with a higher concentration on the substrate tend to agglomerate and are more easily encapsulated by excess carbon, hence becoming inactive in growing SWCNTs (and for spillover catalysis). Hydrogen adsorption isotherms were also measured at 77K

and showed significant differences. Fitting these data using the two-site Fermi-Dirac (Double Langmuir) isotherm based on the assumption of two types of site (groove site and external convex surface site) with different adsorption energies yields excellent fits in both cases and clearly shows that the difference in isotherm shape is due to Sample 2 having fewer of the sites with the higher heat of adsorption (assumed to be the groove sites). First principles calculations of the binding energy of hydrogen molecules were presented which confirm that the adsorption energy at the groove sites is higher than on the exterior surface of tubes, by an amount that increases with increasing tube diameter although the actual values would suggest that the experimental samples have slightly smaller diameter tubes than those simulated in the calculation. This model is entirely consistent with earlier inelastic neutron scattering measurements on a similar sample of SWCNTs. It is therefore to be expected that similar models could be applied to analyse similar experiments on activated carbons, perhaps assuming a Gaussian distribution of trapping energies.

**References**

[1] Murata K, Kaneko K, Kanoh H, Kasuya D, Takahashi K, Kokai F, et al. Adsorption Mechanism of Supercritical Hydrogen in Internal and Interstitial Nanospaces of a Single-Wall Carbon Nanohorn Assembly. J Phys Chem B 2002; 106:11132-11138

[2] Darkrim FL, Malbrunot P, Tartaglia GP. Review of hydrogen storage by adsorption in carbon nanotubes. Int J Hydrogen Energy 2002; 27:193-202

[3] Dillon AC, Heben MJ. Hydrogen storage using carbon adsorbents: past, present and future. Appl Phys A 2001; 72:133-142

[4] Williams KA, Eklund PC. Monte Carlo simulations of $H_2$ physisorption in finite-diameter carbon nanotube ropes. Chem Phys Lett 2000; 320:352-358

[5] Georgiev PA, Ross DK, De Monte A, Montaretto-Marullo U, Edwards RAH, Adams MA Colognesi D. Hydrogen site occupancies in single-walled carbon nanotubes studied by inelastic neutron scattering. Carbon 2005; 43: 895-906

[6] Pantella B, Hirscher M and Ludescher B. Low–temperature thermal-desorption mass spectrometry applied to investigate the hydrogen adsorption on porous solids. Microoporous and Mesoporous Materials 2007; 103: 230-234.

[7] Seifi M, Ross DK, Giannasi A. Raman characterisation of single-walled carbon nanotubes produced by the catalytic pyrolysis of methane. Carbon 2007; 45:1871-1879

[8] Aradi B, Hourahine B, and Frauenheim T. DFTB $^{+}$, A sparse matrix-based implementation of the DFTB method. J Phys Chem A 2007; 111: 5678-5684 .

[9] Elstner M, Hobza P, Frauenheim T, Suhai S, Kaxiras E. Hydrogen bonding and stacking interactions of nucleic acid base pairs: A density-functional-theory based treatment. J Chem Phys 2001; 114: 5149 - 5155.

[10] Riley DJ and Morrison I, to be published.

[11]Kanzow H, Schmalz A, Ding, A. Laser-assisted production of multi-walled carbon nanotubes from acetylene. Chem. Phys. Lett. 1998; 295:525-530

[12] Gregg SJ, Sing KSW. Adsorption, surface area and porosity. Academic Press NY 1967; 121-157

[13] Gundiah G, Govindaraj A, Rajalakshmi N, Dhathathreyan KS, Rao CNR. Hydrogen storage in carbon nanotubes and related materials. J. Mater. Chem. 2003;13:209-213

[14] Wang Q, Johnson JK. Computer simnulation of hydrogen adsorption on graphite monofibres. J Phys Chem B 1999;103:277-281

[15] Ye Y, Ahn CC, Witham C, Fultz B, Liu J, Rinzler G et al. Hydrogen adsorption and cohesive energy of single-walled carbon nanotubes. Appl. Phys. Lett 1999; 74 :2307-2309

[16] Anson A, Jagiello J, Parra JB, Sanjuan ML, Benito AM, Maser WK et al. Porosity, surface area, surface energy, and hydrogen adsorption in nanostructured carbons. J Phys Chem 2004;108 :15820-15826

[17] Bronikowski MJ, Willis PA, Colbert DT, Smith KA, Smalley RE, J. Vac. Sci Technol. A 2001; 19:1800-1805

[18] Panella B, Hirscher M. Raman studies of hydrogen adsorbed on nanostructured porous materials. Phys Chem Chem Phys 2008; 10:2910-2917

[19] Williams KA, Eklund PC. Monte Carlo Simulations of $H_2$ physisorption in finite-diameter carbon nanotube ropes. Chem Phys Letts 2000; 320:352-358.

[20] Henwood D, Carey JD. A*b initio* investigation of molecular hydrogen physisorption on graphene and carbon nanotubes. Phys Rev B 2007; 75:245413 (1-10).

[21] Cabria I, Lopez MJ, Alonzo JA. Hydrogen storage capacities of nanoporous carbon calculated by density functional and Møller-Plesset methods. Phys. Rev. B 2008; 78:075415(1-9)

[22] Okamoto Y, Miyamoto Y. *Ab initio* investigation of physisorption of molecular hydrogen on planar and curved graphenes. J Phys Chem B 2001; 105:3470-3474

**Table Headings**

Table 1. BET Surface Areas, Hydrogen Adsorption (wt%) and fitted heats of adsorption using the Double Langmuir model for the nanotube samples.

Table 2. Calculated binding energies for $H_2$ on different nanotube configurations.

**Figure Captions**

Figure 1. Nitrogen adsorption and desorption isotherms for both samples at 77K following degassing at 720K: (a) sample 1, adsorption (open circles) and desorption (filled circles) with a corresponding surface area of 350 $m^2/g$; (b) sample 2,

Figure 2. Adsorption isotherms for hydrogen on Sample 1 (circles) and sample 2 (squares). Isotherms are plotted on a linear scale in (a) and a double-logarithmic scale in (b) to emphasise the low pressure part.

Figure 3. Hydrogen storage densities of sample 1 (circles) and sample 2 (squares) normalised to the measured BET surface areas as a function of pressure. (a) for linear scale and (b) for a double-logarithmic scale

Figure 4. Adsorption data for hydrogen (open circles) plotted against chemical potential compared with the fit to Equation (4), yielding a single trapping energy of (a) sample 1 (53 meV) and (b) sample 2 (58 meV).

Figure 5. Data for adsorption of hydrogen plotted against chemical potential and fitted with a two-site Langmuir (Equation 5) for (a) sample 1 with heats of adsorption of 53.3 and 39.1 meV and (b) sample 2 with heats of adsorption of 60.8 and 47.7 meV.

Figure 6. Diagrams of the orientations of the $H_2$ molecules for which the calculations were preformed for (a) the surface sites and (b) the groove site

Figure 7. Calculated binding energy of hydrogen molecules as a function of molecule position for single-walled carbon nanotubes for (a) surface sites and (b) groove sites

## CARBON submission checklist

Please check the following points before approving the pdf file for your manuscript.
Defective manuscripts will be returned.

1. Have you read and followed instructions in the Guide for Authors? Pay special attention to section numbering and the required format for references. A Chinese version of the Guide is available on the journal homepage. YES

2. Is an Abstract of less than 200 words included in the manuscript for Review Articles and Research Papers? An abstract of not more that 100 words must be included in the manuscript for Letters. YES

3. Is each reference given a separate number? [12a] not allowed. YES

4. Is the source document typed using only Western fonts and double spaced with a 12 point font size throughout – **including References**?
NOTE: Do not use Oriental fonts. Times New Roman and Symbol fonts preferred. YES

5. Make sure that the pdf file of your manuscript is easy for reviewers to read. For example, figure captions should be clearly separated from the main text and appear on the same page as the figure. YES

6. Make sure you include the carbon in abbreviations (CNF, CNT, MWCNT, SWCNT, ACNT, etc.)
NOTE: English grammar dictates that the abbreviation must refer to the singular. We say “the production of MWCNTs”, but “MWCNT properties”, etc. YES

7. For a Letter to the Editor – is the text, including references, less than FIVE double-spaced pages? AND are there no more than five figures + tables combined? XX

8. Have you provided a list of names and e-mail addresses for at least three suggested **international** (at least two countries) peer reviewers? YES

**AGAIN: READ AND FOLLOW THE GUIDE FOR AUTHORS. A CHINESE VERSION IS**
**AVAILABLE ON THE JOURNAL HOMEPAGE**

**Figure(s)**

Fig 1 (a)

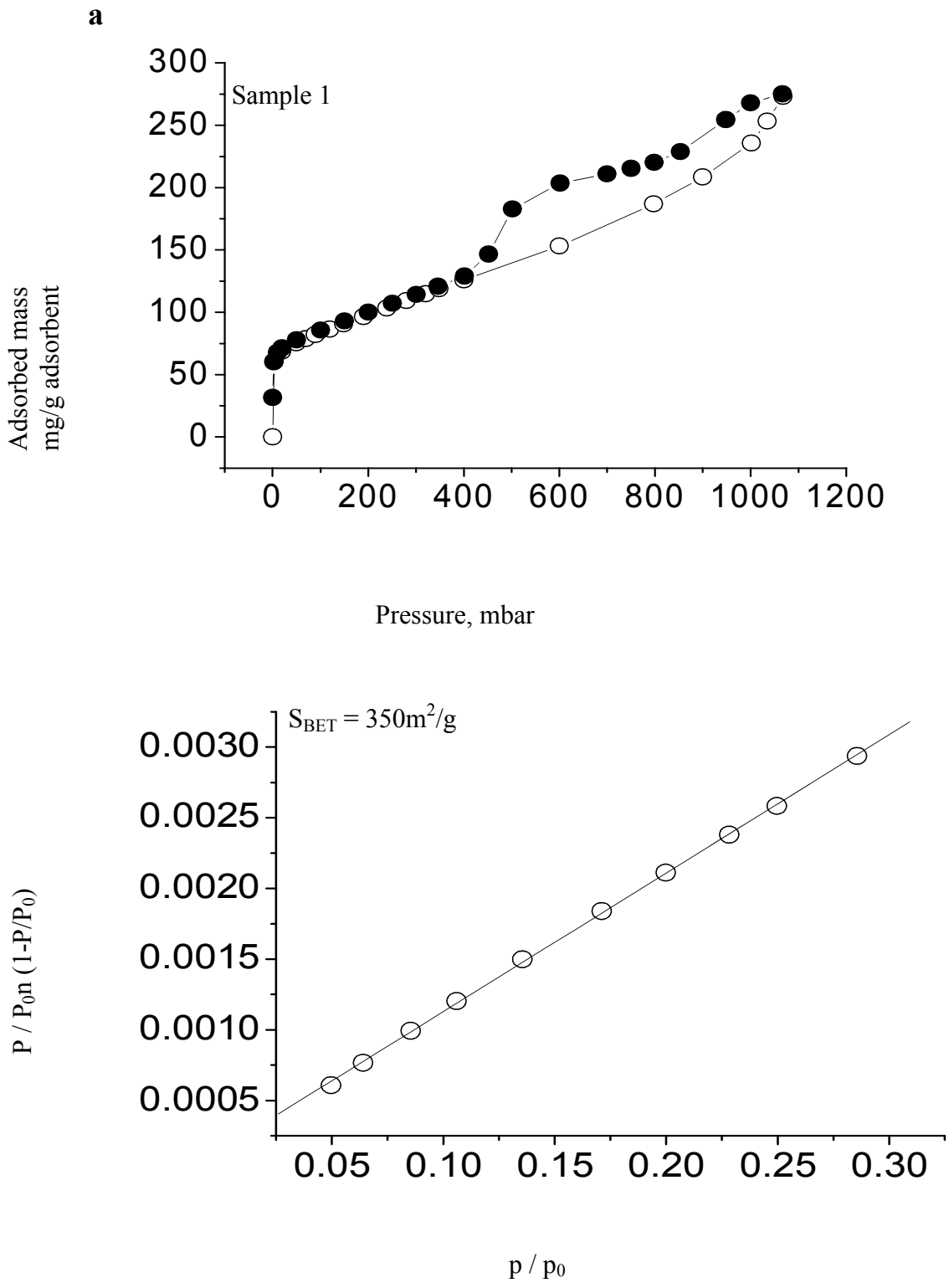

Fig 1(b)

**b**

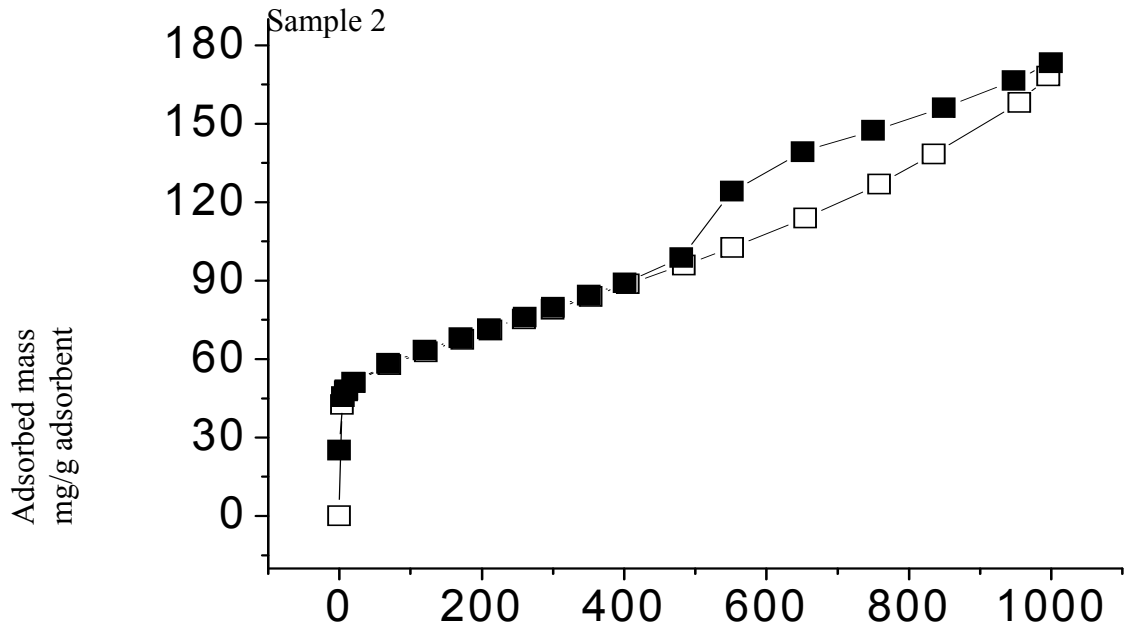
Sample 2
Adsorbed mass
mg/g adsorbent
180
150
120
90
60
30
0
0
200
400
600
800
1000
Pressure, mbar

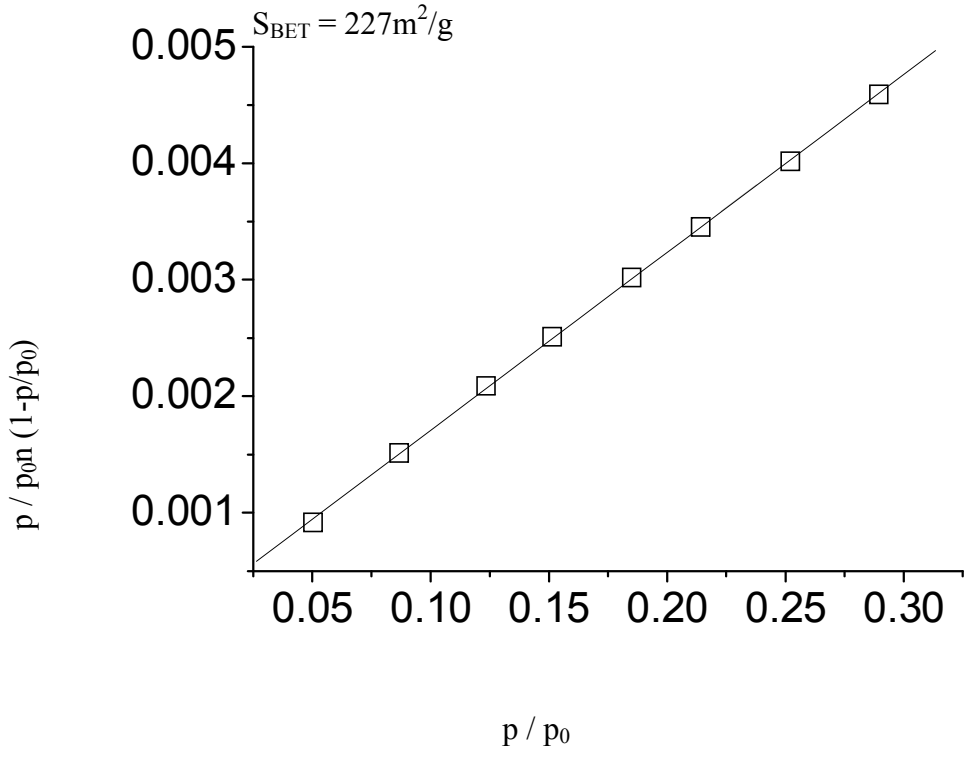
$S_{BET}$ = 227$m^2$/g
p / p0n (1-p/p0)
0.005
0.004
0.003
0.002
0.001
0.05
0.10
0.15
0.20
0.25
0.30
p / p0

Fig 2

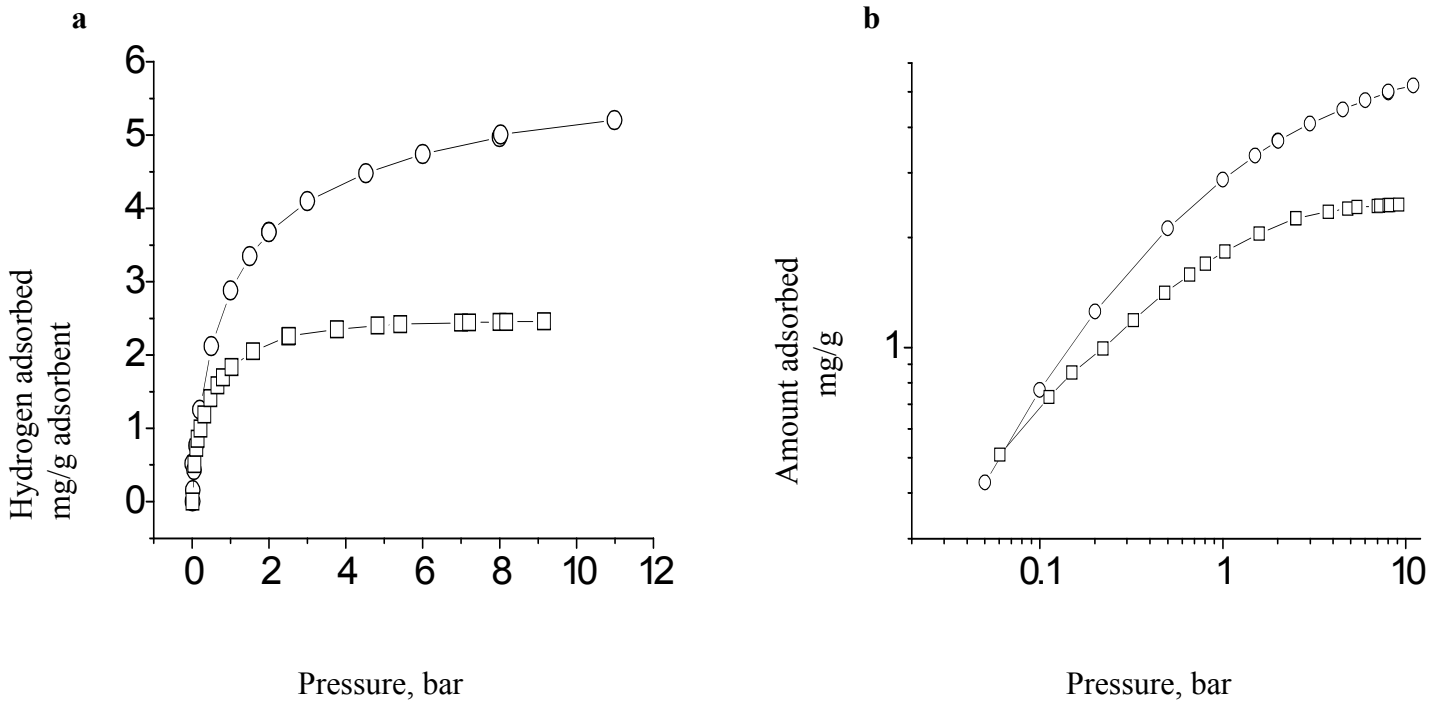
a
b
Hydrogen adsorbed
mg/g adsorbent
Amount adsorbed
mg/g
Pressure, bar
Pressure, bar

Fig 3

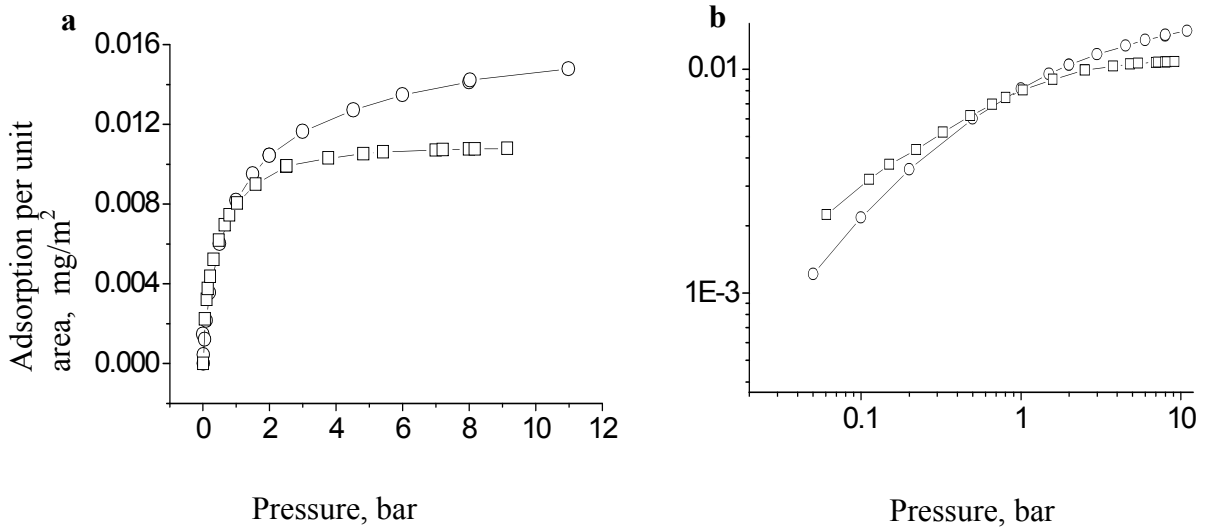
a
b
Adsorption per unit
area, mg/m2
Pressure, bar
Pressure, bar

Figure 4

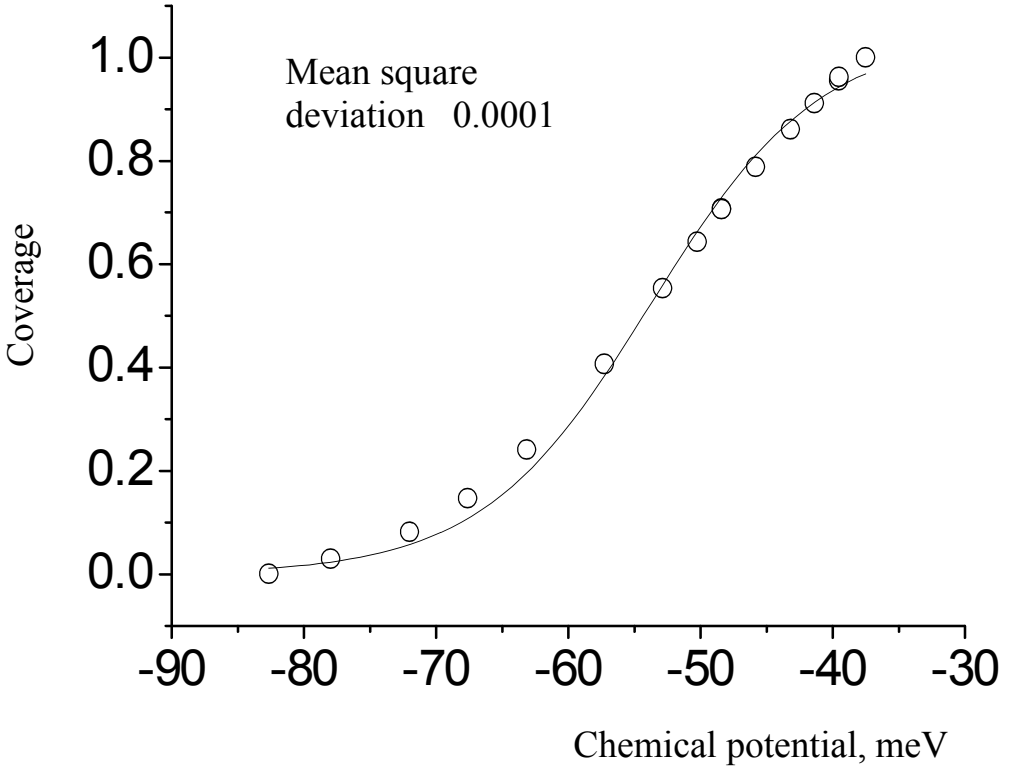
Mean square
deviation 0.0001
Coverage
1.0
0.8
0.6
0.4
0.2
0.0
-90
-80
-70
-60
-50
-40
-30
Chemical potential, meV

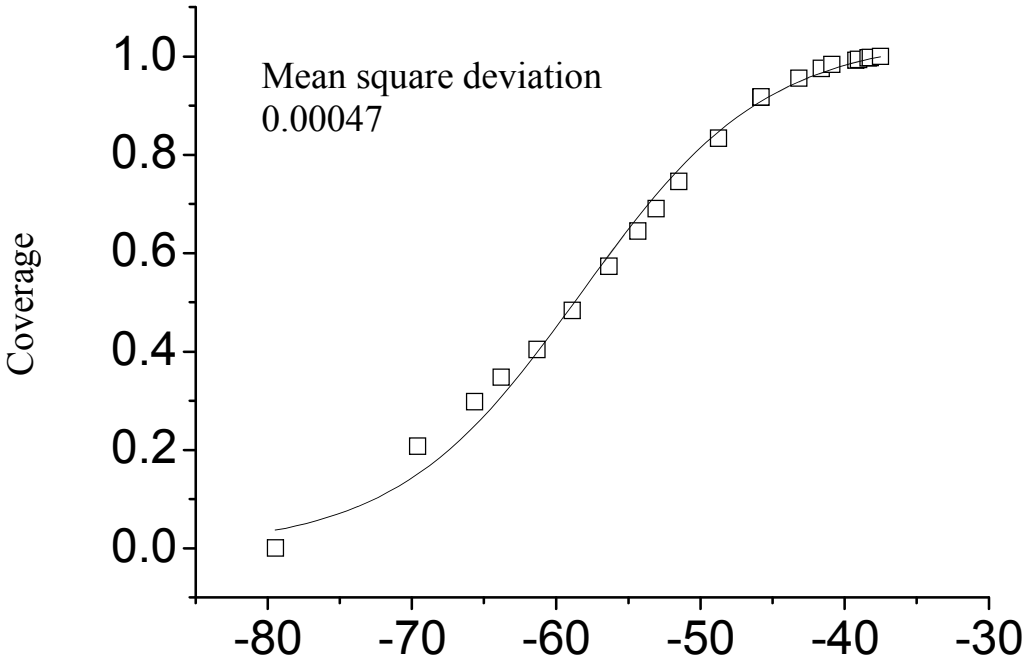
Mean square deviation
0.00047
Coverage
1.0
0.8
0.6
0.4
0.2
0.0
-80
-70
-60
-50
-40
-30
Chemical potential, meV

Figure 5

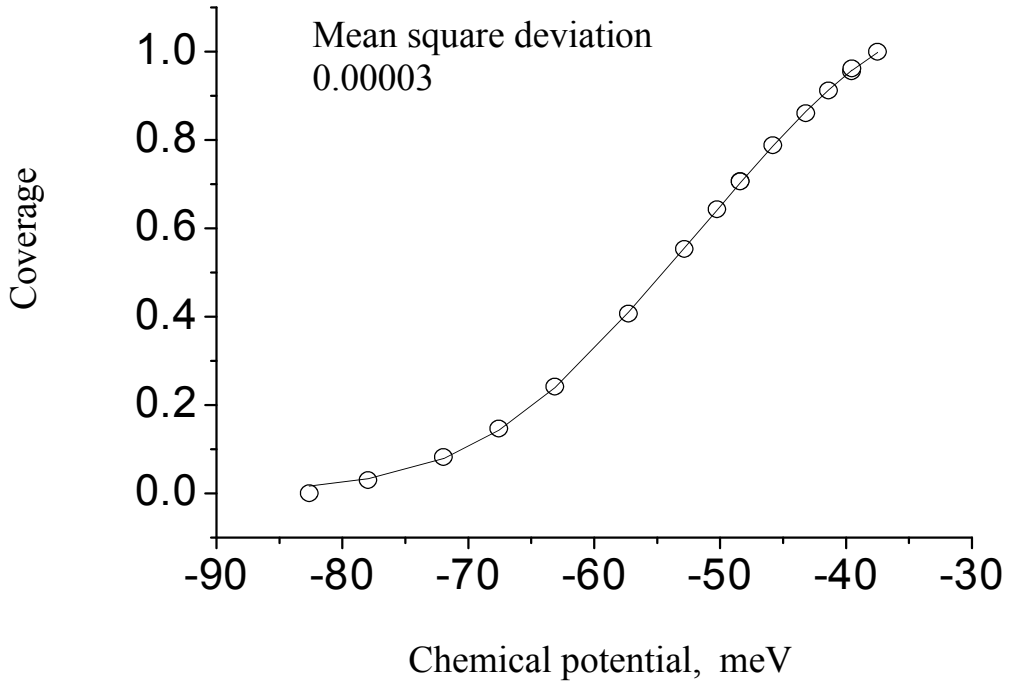
Mean square deviation
0.00003
Coverage
1.0
0.8
0.6
0.4
0.2
0.0
-90
-80
-70
-60
-50
-40
-30
Chemical potential, meV

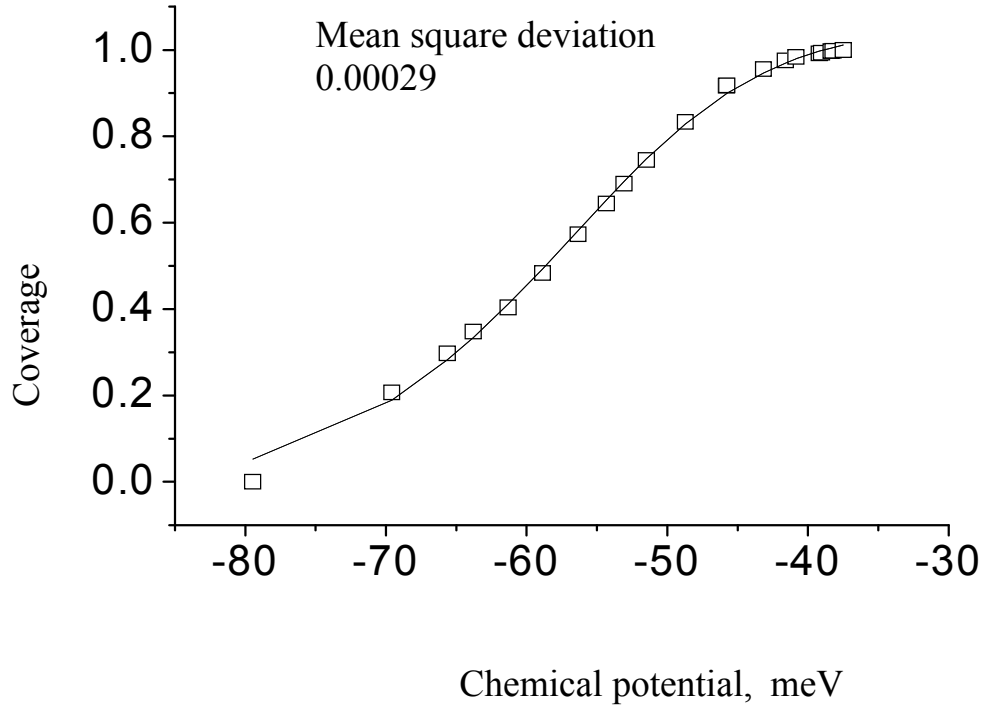
Mean square deviation
0.00029
Coverage
1.0
0.8
0.6
0.4
0.2
0.0
-80
-70
-60
-50
-40
-30
Chemical potential, meV

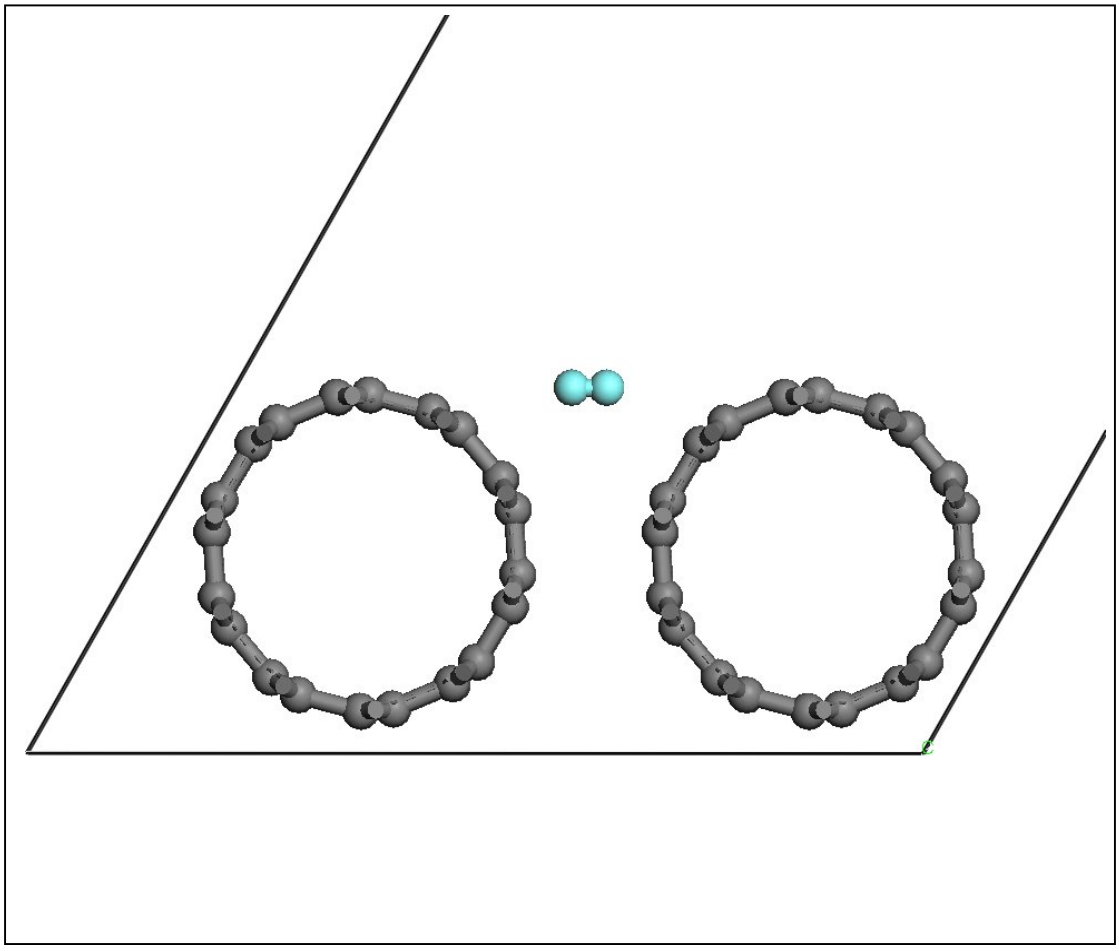

Fig 6

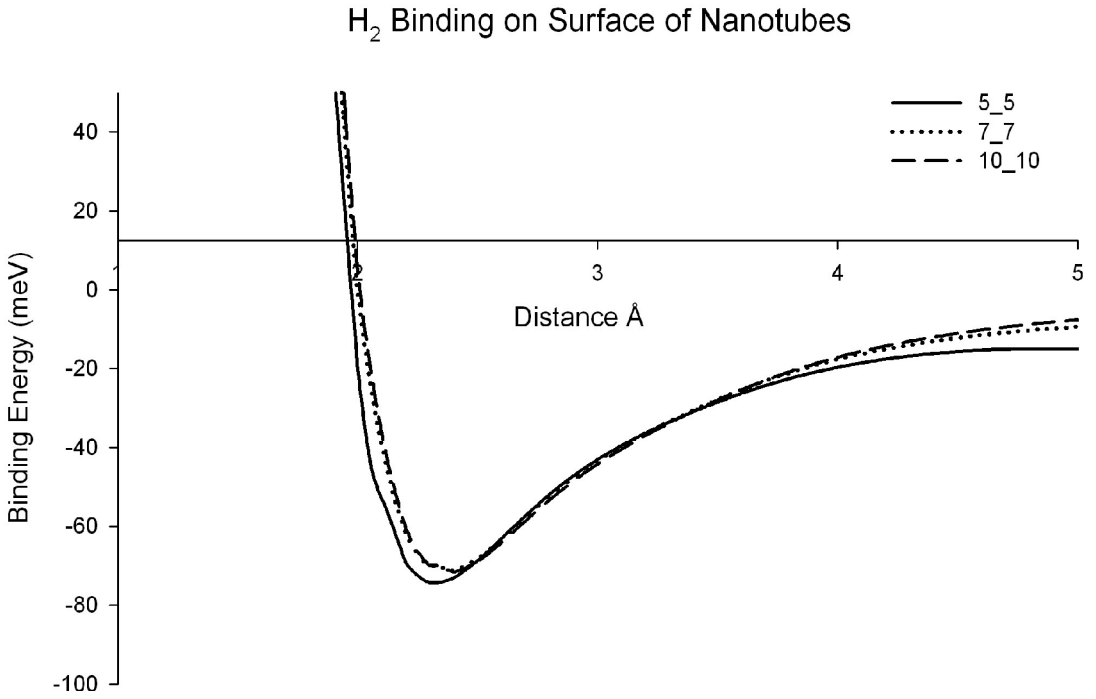
H2 Binding on Surface of Nanotubes
5_5
7_7
10_10
40
20
0
-20
-40
-60
-80
-100
3
4
5
Distance Å
Binding Energy (meV)

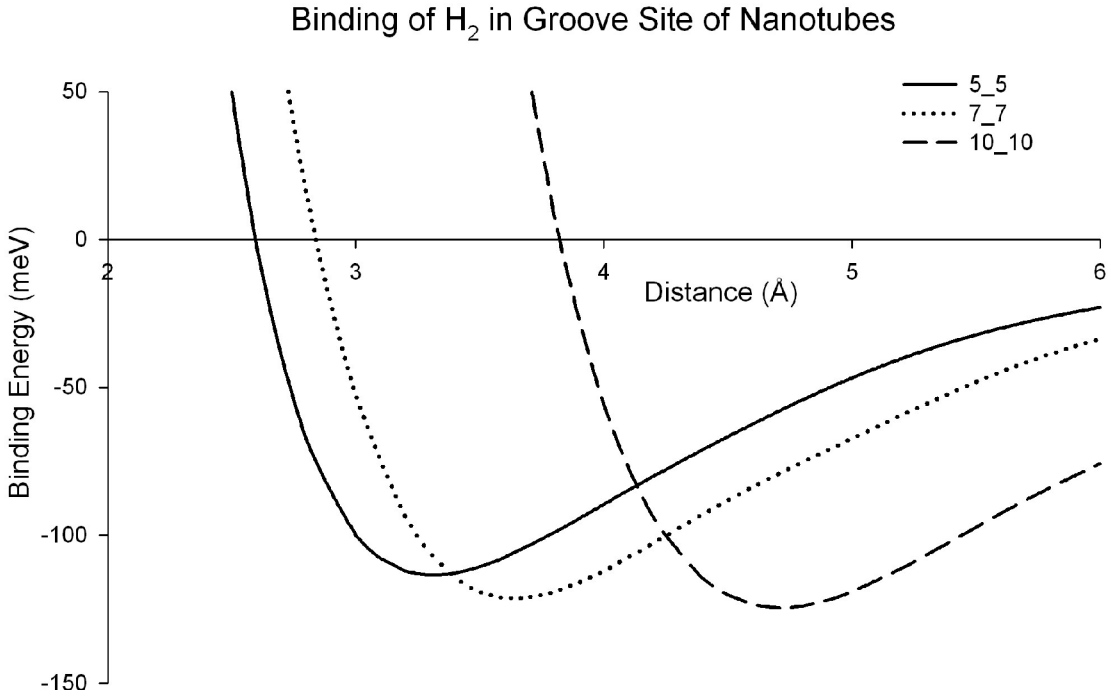
Binding of H2 in Groove Site of Nanotubes
5_5
7_7
10_10
50
0
-50
-100
-150
2
3
4
5
6
Distance (Å)
Binding Energy (meV)

Fig 7

**Tables with mod**

Table 1. BET Surface Areas, Hydrogen Adsorption (wt%) and fitted heats of adsorption using the Double Langmuir model for the nanotube samples

| Material | Surface area, $m^2/g$ at 77 K | Storage capacity wt% at 10 bar | Isosteric heat of adsorption meV/$H_2$ | Proportions stored in each site, % |
|---|---|---|---|---|
| Sample 1 | 350 | 0.5 | -53.3 ±0.8<br>-39.1 ±1.2 | 40<br>60 |
| Sample 2 | 227 | 0.25 | -60.8 ±4.8<br>-47.7 ±1.8 | 30<br>70 |

Table 2. Calculated binding energies of $H_2$ on different nanotube configurations. The Effective Binding Energy is the Binding Energy less the Zero Point Energy.

| Tube/Site | Binding Energy (meV) | Zero Point Energy (meV) | Effective Binding Energy (meV) |
|---|---|---|---|
| **5_5 Groove** | 113.54 | 24.47 | 89.07 |
| **7_7 Groove** | 121.21 | 29.78 | 91.43 |
| **10_10 Groove** | 124.54 | 24.88 | 96.66 |
| **5_5 Surface** | 74.30 | 18.40 | 55.90 |
| **7_7 Surface** | 71.35 | 14.91 | 56.44 |
| **10_10 Surface** | 71.67 | 15.43 | 56.24 |